Atomic Spectroscopy

Article

Uptake and Translocation of ZnO Nanoparticles in Rice Tissues Studied by Single Particle-ICP-MS

Hao Cui,[a, b] Zixuan Zhang,[c] Tianyu Wang,[a] Jiayi Hong,[a] Lidan Lei,[d] and Shiqiang Wei[a, *]

[a] College of Resources and Environment, Department of Environment Science and Engineering, Southwest University, Chongqing 400715, P. R. China

[b] Key Laboratory of Testing and Tracing of Rare Earth Products for State Market Regulation, Jiangxi University of Science and Technology, Ganzhou 341000, P. R. China

[c] Key laboratory of Luminescence Analysis and Molecular Sensing (Southwest University), Ministry of Education, College of Pharmaceutical Sciences, Southwest University, Chongqing 400715, P. R. China

[d] Chongqing Key Laboratory of Karst Environment, School of Geographical Sciences, Southwest University, Chongqing 400715, P. R. China

Received: *September 05, 2023;* ***Revised:*** *November 23, 2023;* ***Accepted:*** *November 23, 2023;* ***Available online:*** *November 23, 2023.*

DOI: 10.46770/AS.2023.202

ABSTRACT: Foliar spay of zinc oxide nanoparticles (ZnO-NPs) is a common practice to provide the necessary Zn element for crops, which may also be a potential source for human expose to NPs with possible adverse health effects. Presently little is known about the forms and distributions of ZnO-NPs in plants after it is applied by foliar spay due to the lack of reliable quantification method. In this work, a complexed enzymatic extractant combined with single particle-ICP-MS system (SP-ICP-MS) was developed for simultaneously determining the concentrations and size distributions of ZnO-NPs in plant tissues. The measuring conditions were optimized and the method was applied to quantify ZnO-NPs uptake and distributions in rice plants after foliar application of ZnO-NPs. The results showed that the established method could well quantify the NP concentration in plant tissues with a detection limit of 16 nm; foliar spray of ZnO-NPs increased the Zn concentration (22.66 ± 0.51 $mg \cdot kg^{-1}$) in rice grains by 447%, which was still within the limits of the food safety standard of China (NY 861-2004, 50 $mg \cdot kg^{-1}$ for Zn). ZnO-NPs larger than 60 nm cannot be directly absorbed by the leaves and may instead fall into the soil. ZnO-NPs with a size between 30-60 nm in the leaves could be retained due to the hindering effect of the cellulose-hemicellulose network. The smaller ZnO-NPs with size less than 30 nm could only be detected in stems but not in the grains, indicating that ZnO-NPs were dissociated or resolved as ionic form before they were transported into grains. The xylem and phloem were believed to be the organs responsible for the translocation and transformation of ZnO-NPs after being uptake by rice leaves. The study demonstrated the feasibility of the proposed method in characterizing NP behaviours in plants and proved the effectiveness and safety of foliar application of ZnO-NPs to rice.

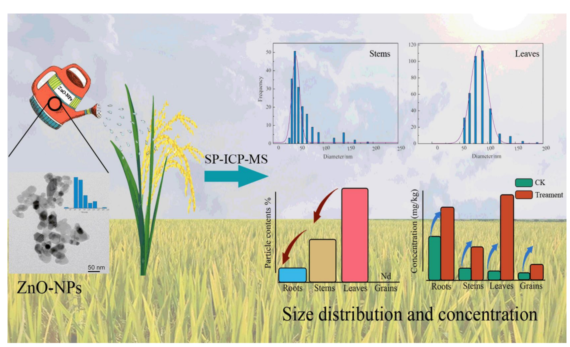

INTRODUCTION

More than 50% of global paddy suffer from a zinc-deficiency problem, leading to reduced rice yields and Zn-deficient rice grains.[1] A traditional strategy for resolving this issue is to apply Zn-containing fertilizers to soils.[2] However, Zn ions can easily combine with clay minerals in the soil matrix, thereby decreasing its bio-availability to crops.[3] Therefore, the foliar spray of Zn-fertilizers is increasingly applied for alleviating Zn deficiencies in crops.[4, 5]

The ZnO nanoparticles (ZnO-NPs) are used as a new type of foliar fertilizer to mitigate zinc deficiency in rice in recent years, which can be absorbed by rice leaves and stored in rice tissues for slow release, providing essential Zn elements for rice growth.

Some researchers pointed out that the absorption and transport of ZnO-NPs in rice was directly related to its particle size, concentration, and aggregation. For example, Avellan *et al.* [6] and Kah. *et al.*[7] claimed that nearly 100% of NPs with sizes of approximately 3 nm could be transferred into wheat leaves, whereas those with sizes of over 50 nm were almost entirely washed off by rain, while T. Eichert. et al. and A. B. Bombo.et al. had been proposed that NPs with sizes of 8-60 nm were easily taken up by leaves.[8, 9] The differences in the absorbable particle sizes obtained by different authors might come from the differences in analysis and testing methods. Although foliar spay of ZnO-NPs has been proved to be an efficient way to supply Zn nutrient for rice growth, it might pose a potential risk for human health, depending on the concentration and size of the NPs in rice plants, especially in grains. Therefore, it is necessary to develop an analytical technique for the accurate qualitative and quantitative analyses of the concentration and distribution of NPs in rice tissues.

Microscopy techniques including scanning electron microscopy (SEM) and transmission electron microscopy (TEM) are commonly employed to observe the size and morphology of NPs in plants.[10, 11] However, most of microscopic imaging techniques have limitations in qualitative and quantitative measurements of NPs in plants. For instance, SEM or TEM in combination with the near edge X-ray absorption fine structure analyses have been adopted to determine the elemental composition of NPs, while the results are usually semi-quantitative.[12] Additionally, NPs usually exist in plants in trace levels ($\mu g \cdot kg^{-1}$ to $mg \cdot kg^{-1}$), which makes their direct measurement by TEM or SEM a big challenge. Dynamic light scattering (DLS) is also widely used for investigating the diffusion behaviour of macromolecules and size distributions in solutions,[13] while it is not suitable for particles with significant size variations (up to three orders of magnitude for foliar agents) . In addition, it is well known that the physico-chemical properties of metals and their oxides in NPs forms are completely different from their none-NP forms, NPs may have potentially negative effects on human health regardless of original chemical properties.[14] Hence, quantitative analyses of NPs in crops are critical for food safety assessment. Most traditional solution nebulization sampling techniques (such as atomic absorption spectroscopy (GFAAS), inductively coupled plasma optical emission spectroscopy (ICP-OES), and inductively coupled plasma mass spectrometry (ICP-MS) have limitations in the quantification of metal NPs in plant tissues.[15-31] In particular, they cannot distinguish between Zn^{2+} and ZnO-NPs signals, leading to significant bias.[32]

Compared with traditional ICP-MS, single particle ICP-MS (SP-ICP-MS) enables the qualitative and quantitative analyses of target analytes (including their particle size distribution) in biological and environmental samples.[33-37] The SP-ICP-MS combines a “single particle” mode with traditional ICP-MS. This mode represents a computational function, which sets a relatively short dwell time and continuously records pulse signals while introducing individual metal-based NPs into the instrument.[38] This approach allows an easy calculation of particle size distributions and NPs concentrations.[39] Hence, the SP-ICP-MS technique possesses low concentration detection limits and the ability to determine the NPs composition. It can also derive a nanoparticle size distribution from the particle signal intensity. In a word, these remarkable capabilities of SP-ICP-MS make it a powerful method for monitoring the bio-transfer of NPs in plant tissues. However, the extraction of NPs from plant tissues without compromising their properties is an unprecedented challenge.

Traditional acid or alkali digestion are commonly used for metal extraction from plant tissues; however, they are not suitable for NPs analyses as the concentrated acids can dissolve the NPs into ionic forms. Enzyme digestion might be a reliable measure for the pre-treatment of NPs analyses due to its mild conditions. Wei *et al.*[40] used Macerozyme R-10 enzyme to extract Au-NPs from leaves of lettuce plants. However, the cellulose content in rice was significantly higher than that in lettuce plants, and its tissue composition was more complex. Therefore, a single enzyme was not sufficient for extracting NPs from the xylem in rice. For complex tissues, to extract NPs in the different plant tissues, Laughton *et al.*[41] employed a three-step extraction process involving three reagents, including MeOH, Tween-80, and enzymes. However, the multi-step extraction technique led to particle loss and contamination. Hence, the complex enzyme system, as a digestion extractant, has potential ability to extract NPs from rice tissues without alteration of their original occurrence.

Herein, we developed a complex enzyme digestion system combined with SP-ICP-MS for the measurement of the ZnO-NPs size distributions and concentrations in plant tissues (roots, leaves, stems, and grains), and the uptake and accumulation of ZnO-NPs by rice after its foliar spray were investigated based on the established method.

EXPERIMENTAL

Materials. Ultrapure water (18.2 $M\Omega \cdot cm^{-1}$), obtained by a Millipore water system (Merck the Millipore, Fontenay-sous-Bois, France), was used for the preparations of all the sample solutions. The standard $Zn(NO_3)_2$ solution containing 1000 mg $Zn \cdot L^{-1}$ was purchased from the National Centre for Analysis and Testing of Steel Materials (Beijing, China). The ZnO-NPs standard suspensions (containing 100 mg $ZnO \cdot L^{-1}$) with particle sizes of 30-100 and 50 ± 10 nm, as well as the Au NPs standard suspensions (50 ±10 nm, 0.05 $mg \cdot L^{-1}$, and 1×10^7 $particles \cdot mL^{-1}$) were all purchased from the Aladdin Biochemical Technology (Shanghai, China). The Au NPs standard suspensions was diluted to 1×10^5

particles·mL^{-1}, using 5 mmol·L^{-1} sodium citrate as a dispersant, which was used to measure the transport efficiency (TE%) of nano-particles. NexION setup solution (N81450510, containing 1 μg·L^{-1}, Be, In, Ce, and U) was from PerkinElmer. Hydrochloric acid (HCl) and nitric acid (HNO_3) of guaranteed reagent grade was procured from Sinopharm Group (Shanghai, China). The HCl and HNO_3 were further purified by an infrared acid purification system. Macerozyme R-10 enzyme (CAS: 9032-75-1) and Carbohydrate-active enzymes (CAS: 9012-54-8) (named compound enzyme) were purchased from Zheye Biochemical technology (Shanghai, China), using for the digestion of roots, leaves, stems, and grains. Additionally, the mixed extraction buffer [42] (50 mmol·L^{-1} Trizma HCl (Tris-HCl, ≥99.0% (titration)), 250 mmol·L^{-1} sucrose, 1.0 mmol·L^{-1} Dithioerythritol (DTE, $C_4H_{10}O_2S_2$, ≥99.0%, Sigma D8255), 5.0 mmol·L^{-1} ascorbic acid and 1.0% w:v Polyclar AT (PVPP, ≥99.0%) came from the Bailin-Wei Scientific (Beijing, China) were used throughout the pre-treatment process. All the other chemicals involved were of guaranteed reagent grade. All the glassware and PET battles were soaked by 10% HNO_3 for 48 h. These materials were then rinsed with ultrapure water three times.

Experimental design and treatment procedure. A surface calcareous purple soil sample (0-20 cm) was collected by wooden spades from a Zn-deficient paddy at the National Monitoring Station of Soil Fertility and Fertilizer Efficiency on Purple Soils, Beibei, Chongqing, China. The total amount of 100 kg purple soils was sampled in match of the need for the pot experiments. which was air-dried after the removal of plant residues and gravels, then ground, mixed, and passed through 2 mm nylon sieves priori to use. The total and bioavailable Zn contents of the tested soil were 25.2 and 1.12 mg·kg^{-1}, respectively. Other relevant soil properties are listed in Table 1.

Pot experiments were carried out in a greenhouse at Southwest University, China, to investigate the uptake and transport of ZnO-NPs in rice plants after foliar spay. Each plastic pot was filled with 10 kg of the prepared soil and chemical fertilizers including urea (0.83 g·kg^{-1}), P_2O_5 (1.00 g·kg^{-1}), and K_2O (0.15 g·kg^{-1}) were applied as basic nutrients. De-ionized water was added to each pot to keep flooded conditions (2 cm above the soil surface) for 30 d. Then, two rice seedlings (Yi-you 2108) with three leaves were transplanted into each pot, which was kept flooded (5 cm) until the harvest stage. Three treatments were set as the control (de-ionized water, CK), foliar spay of ZnO-NPs with size of 30-100 nm and those with size of 50 ± 10 nm. The 10 mol·L^{-1} ZnO-NPs suspension (5 mL per exposed plant) was sprayed on rice leaves in treated groups. Nine pots in three replicates were randomly arranged to exclude the environmental influences. The foliar spay was conducted at the tilling stage of rice growth, approximately two months after transplanting rice seedlings. Afterward, each of one rice plant from the three replications of same treatment were sampled entirely at elongation stage and maturation stage to form a mixed sample for each treatment. The fresh plants were rinsed

Table 1. Basic soil properties n=5

Paddy property	Values
pH	8.21 ± 0.11
Organic matter, g·kg^{-1}	34.6± 0.23
Water-soluble nitrogen, mg·kg^{-1}	209± 12
EC, dS·m^{-1}	0.28± 0.05
N, mg·kg^{-1}	21.1± 0.42
P, kg·ha^{-1}	16.8± 0.21
K, kg·ha^{-1}	321.8± 53
Total Zn, mg·kg^{-1}	25.2± 0.27
Bio-Zn, mg·kg^{-1}	1.12± 0.17

Table 2. Optimized parameters of ICP-MS and SP-ICP-MS

ICP-MS		
Nebulizer	Concentric plus glass, type C	
Spray chamber	Cyclonic Spray chamber	
Nebulizer gas flow, L·min^{-1}	1.04^a	
Auxiliary gas flow, L·min^{-1}	1.2	
Plasma gas flow, L·min^{-1}	16	
RF power, W	1550	
Sampler/Skimmer cones	Nickel	
Target ions	^{11}B, ^{27}Al, ^{111}Cd, ^{59}Co, ^{57}Fe, ^{55}Mn, ^{208}Pb, ^{88}Sr, ^{75}As, and ^{66}Zn	
SP-ICP-MS		
Monitored isotope, m/z	^{66}Zn	^{197}Au
Dwell time, μs	100^a	
Scan time, s	140	
Density, g·cm^{-3}	7.14	19.3
Mass fraction, %	100	100
Ionization efficiency, %	100	100
Rpa	0.5	

^{a} Default conditions

by 0.5% HNO_3 and washed by deionized water to thoroughly remove the possible impurities, then the plants were divided into various tissues including roots, stems (stem nodes) and leaves (flag leaves and downward leaves) and grains (mature stage). All the plant tissue samples were kept in a refrigerator at -80°C until the element and NPs analyses, then they are dried by oven (80°C overnight) and grounded to pass a sieve with pore size of 80 mesh for analyses.

Optimization of the SP-ICP-MS for the measurement of ZnO-NPs in plant. The rice tissues (roots, leaves, stems, and grains) were digested with the compound enzyme system at pH 6.5-7.5 for 48 h to extract ZnO-NPs from the rice tissues. A detailed description of the extraction process is provided in Supporting Information. After the compound enzyme extraction, the samples were divided into two sub-groups. One set of samples was subjected to the analyses of B, Al, Cd, Co, Fe, Mn, Pb, Sr, As, and Zn contents using conventional ion mode by ICP-MS (NexION 1000G, PerkinElmer, USA), while the concentration of Mg, K, Ca, and P were analysed by ICP-OES (Optima 2000 DV, PerkinElmer, USA). The default ICP-MS and ICP-OES parameters are listed in Table 2 and Table S1, respectively. The other set was subjected to the determination of ZnO-NPs sizes and numbers using a single-particle mode (Syngistix, version 1.0), the default SP-ICP-MS parameters are listed in Table 2. *For accurate analyses* of ZnO-NPs in rice plant, some parameters, including the *nebulizer gas,* sample flow rates, dwell times, and ultrasonication time, were optimized. Firstly, daily performance (*i.e.*, torch alignment, nebulizer gas, QID standard, and standard performance) in normal testing was assessed by observing Be, In, U, Ce, CeO, and background (m/z of 220), which were better than the recommended values by the manufacturer. Then transport efficiency (TE%) and sample flow rates were calculated under optimal conditions using a 50 nm Au-NPs standard solution, and a suspension at 1 $\times 10^5$ particles·mL^{-1}, while the dwell times and ultrasonication time were optimized to realize the presence of (50 ± 10 nm) ZnO-NPs standard solution. Finally, the sample flow rates were defined by standard nano solution and weighing the standard solution after and before aspiration at the selected pump speeds. The TE% values were automatically displayed by single-particle mode (Syngistix, version 1.0). Additionally, to determine the size distribution of ZnO-NPs, Zn^{2+} solutions with concentrations of 0.1-100 μg·L^{-1} were utilised to calculate the pulse intensity-to-mass ratio. The mass ratio of Zn in ZnO was 80.25%, and ZnO particles were assumed to be of spherical shapes with a density of 5.7 g·cm^{-3}. The Syngistix™ Nano application software (PerkinElmer, USA) was used to calculate ZnO-NPs sizes and concentrations. TEM (FEI Tecnai G2 F30, USA) was employed to observe the structure and sizes of the prepared ZnO-NPs.

Effect of compound enzyme system on the extraction of ZnO-NPs. The ZnO-NPs (30-100 nm) were prepared in the compound enzyme solution used for rice tissues digestion and were shaken at a pH 6.5-7.5 for 48 h. The samples were then diluted 50-fold with deionized water for SP-ICP-MS analysis. Compared with the compound enzyme group, the ZnO-NPs (30-100 nm) were also diluted 50-fold with deionized water and were analysed by SP-ICP-MS. All analyses were conducted in triplicate. According to the previous literature, the two commercial sizes of ZnO-NPs, as described above, were characterized by TEM to verify the accuracy of the size distribution by the SP-ICP-MS method.

Data analysis. The original ICP-MS signal intensity (counts or cps) and dwell time were used to calculate a target particle size (for only a single element because the settling time was zero) assuming that the NPs density was constant throughout the process. And that all NPs were spherical. Therefore, NPs sizes were computed via the following three equations [43-45]:

$$\mathrm{W}=\eta_{\mathrm{n}}\times \mathrm{q}_{\mathrm{liq}}\times t_{dt}\times \mathrm{C}\times 10^{-3} \qquad (i)$$

where W (μg·s^{-1}) is a mass flow rate, η_n is a transport efficiency, q_{liq} (mL·s^{-1}) is the sample flow rate, t_{dt} (ms·event $^{-1}$) is the dwell time, and C (μg·L^{-1}) is a sample concentration.

$$m_{NPs} = f_M^{-1} \times \left[\frac{(I_{actual} - I_{Bkgd})\times \eta_{\mathrm{n}} - b}{k}\right] \qquad (ii)$$

where m_{NPs} is a particle mass of NPs, mass fraction (f_M^{-1}) of the particle, I_{actual} (individual pulse intensities) and I_{Bkgd} (minus the average background intensity) are the signal intensities obtained after introducing metal-based NPs, and k is the slope of the calibration curve.

$$d_{NPs} = \sqrt[3]{\left(\frac{6\times m_{NPs}}{\pi \times \rho}\right)} \qquad (iii)$$

where ρ and d_{NPs} are the NPs density and diameters, respectively.

The Origin 8.5 and SPSS Statistics 21 software packages were used for data statistical analyses, and the Spearman ANOVA-Duncan software was utilised for analysing statistical differences between the results obtained among various treatments. The multivariate statistical analyses of the results were carried out using principal component analysis (PCA) through Python 3.10.5.

RESULTS AND DISCUSSION

Optimization of SP-ICP-MS parameters. To maximise the transport efficiency of the SP-ICP-MS method, the ICP-MS uptake speed and gas composition were optimised. The concentration of commercial Au-NPs (50 nm, 1×10^5 particles·mL^{-1}) calculated from the total Au content and their size were 49.78 ± 0.56 μg·L^{-1} and 52 ± 5 nm, respectively. The transport efficiency was computed via the following equation:

$$\eta_{\mathrm{n}} = \frac{f(I_P)}{\mathrm{q}_{\mathrm{liq}} \times N_p} \qquad (vi)$$

where N_p is the number of particles, and $f(Ip)$ is the measured pulse frequency.

As shown in Fig. 1 and Eq. (vi), the transport efficiency of ^{197}Au from Au-NPs with a sodium citrate matrix was studied at sample flow rates between 0.1 and 1.0 mL·min^{-1} and nebulizer flow rates between 0.9 and 1.1 L·min^{-1}. With the increase of the nebulizer flow rate, the transport efficiency also increased (Fig. 1a). However, a diffusion-convection effect likely increased the number of incompletely ionised species during ion transport. When the nebulizer gas flow rate exceeded the optimum value, the oxide ratio exceeded a certain limit ($<$0.025),[46] the Zn isotopes would be subjected to interferences from various Ti, V, and S oxide or hydroxide ions.[47] Hence, the flow rate of the nebulizer gas could not be increased continuously. As shown in Fig. 1b, the sample flow rate is negatively correlated with the transport efficiency.

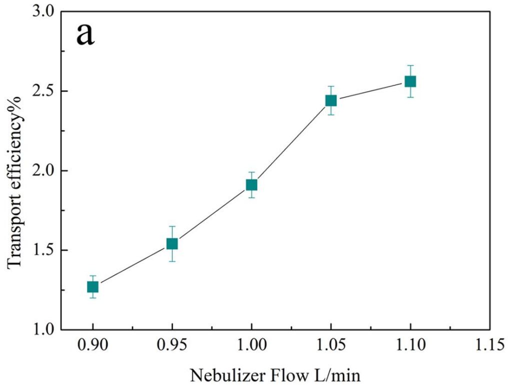

Fig. 1 Effects of SP-ICP-MS parameters on the transport efficiency of commercial Au-NPs (50 nm): (a) nebulizer and (b) sample flow rates.

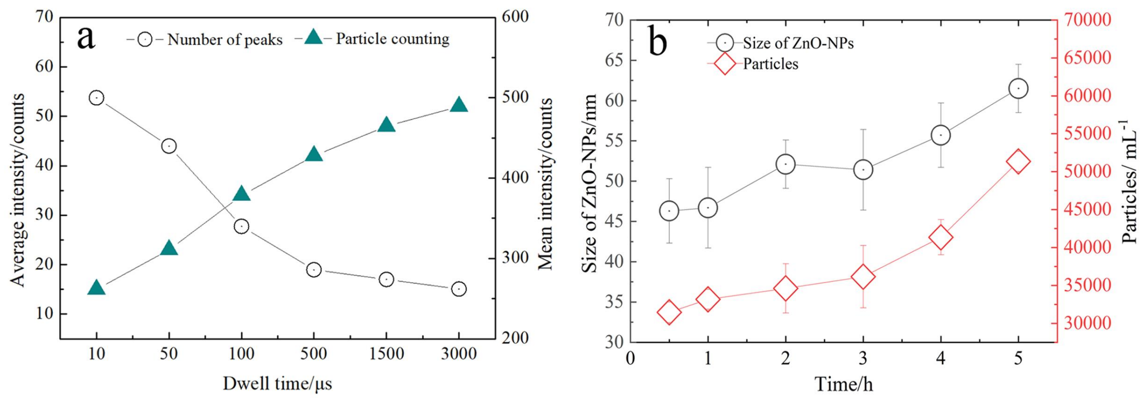

Fig. 2 Effects of SP-ICP-MS parameters on the average number of counts obtained for ZnO-NPs (50 nm): (a) dwell time and (b) ultrasonication time.

However, a low sample flow rate might cause memory effects or nanoparticle agglomeration.[48] According to the graph, the highest transport efficiency of NPs was achieved at a nebulizer flow rate of 1.05 L·min^{-1} and sample flow rate of 0.3 mL·min^{-1}.

Compared with traditional ICP-MS, the SP-ICP-MS signal is generated at a shorter dwell time (usually between 10 and 3000 μs) and represents a function of time.[49] According to the first assumption, each pulse is stranded for a single particle event within a short dwell time at the optimal sample flow rate and adequately low number of particles.[50] Hence, pulse frequency is only correlated to NP concentration. Pulse intensity is positively correlated with the number of particles, particle size.[51] The relationship between the analytical concentration, C (μg·L^{-1}), pulse intensity Q, and particle mass per event (μg·event^{-1}) is expressed by the following formula [52]:

$$Q = \eta_n \times q_{liq} \times t_{dt} \times C \qquad (vii)$$

where t_{dt} represents the dwell time.

In this work, the dwell time of the original ICP-MS systems was set to be 1-5 ms. The SP-ICP-MS system required acquisition times as fast as 10-1000 μs to effectively distinguish small particles. When a whole particle appears within the dwell time, the specific intensity of the particle with respect to that of the ionic background increases, producing a sufficiently large pulse within a shorter dwell time.[53] As shown in Fig. 2a, within the shorter range of dwell time, the number of nanoparticle peaks decreases with the increase of dwell time, while the average peak intensity increases with the increase of dwell time. To reduce the probability of detecting two or more nanoparticles within one unit of dwell time, the optimal dwell time is selected to be 100 μs.

In general, NPs tend to agglomerate and increase their average size. However, the dissolved analyte elements as a difficulty can interfere with nanoparticle size in nanoparticle detection. Hence, ultrasonic pre-treatment is typically performed to disperse NPs. As shown in Fig. 2b, the signal intensity of NPs increases with increasing ultrasonication time and stabilises between 1 to 4 hours of treatment. After 4 hours, the particle size and number of particles of NPs showed an upward trend with the increase of ultrasonic time, and it might be due to Zn ions dissolving on the surface of ZnO-NPs. Hence, the optimal ultrasonication time was selected to be 1 h.

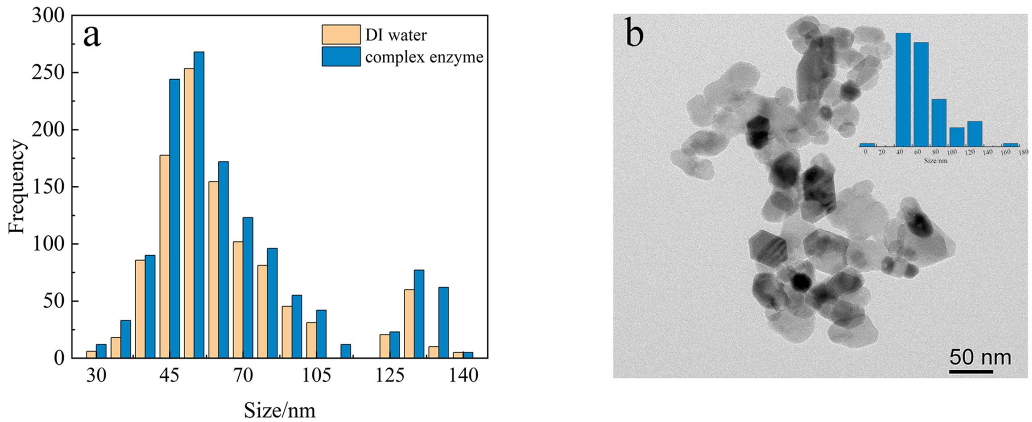

Fig. 3 (a) ZnO-NPs size distributions in the control and treatment groups. (b) TEM images of commercial ZnO-NPs and their size distribution obtained by SP-ICP-MS.

Performance of the SP-ICP-MS method. The limit of detection (LOD) is an essential parameter in analytical chemistry. Previously, its magnitude was calculated as the average signal intensity of the black matrix and 3σ threshold. Le *et al.* [54] suggested that the minimum particle size could be determined from the obtained SP-ICP-MS signal using the quantile of the standard normal distribution. Hence, a 3σ threshold method [55] was employed in this work to distinguish a particle signal from the background signal (Fig. S1) and iteratively calculate the average+3σ threshold until no additional particle signals were detected. Therefore, only at a sufficiently low background noise, the 3σ threshold assumed a low value. We used a sample matrix with an extracting solution factor of 1000 as the background signal generated by SP-ICP-MS for ZnO-NPs.

$$\text{Size of LOD} = \sqrt[3]{\frac{6 \times 3\sigma}{R \times f_{Zn} \times \rho \times \pi}} \qquad (viii)$$

where R (counts·μg^{-1}) is the sensitivity of the detector for a given element, and f_{Zn} is the mass fraction of Zn in ZnO.

According to the original pulse signal intensity and Eq. (i, ii, iii, and viii), an approximate particle size LOD was 14 nm. Some studies reported the detection of ZnO-NPs with sizes of 20-80 nm.[4, 56, 59] Moreover, the smallest detectable size of ZnO-NPs by SP-ICP-MS was 16 nm,[41] which was similar to the value of 14 nm obtained in this work. Because the detectable NP sizes reported previously exceeded this magnitude, it was most likely the lowest particle size LOD.

The number concentration detection limit is related to the ability to count three nanoparticle events, which can be directly linked to the number concentration detection limit (LOD_{number}):

$$LOD_{number} = 3 \times \frac{1}{\eta_{neb} \times \text{qliq} \times t_i} \qquad (viiii)$$

Where η_{neb} is the analyte transport efficiency; t_i is the total acquisition time.

According to Francisco Laborda, *et al.* [56] and Eq.(viiii), the detection limit of number concentration was calculated to be 2.36×10^5 numbers·g^{-1} in our work.

Effect of complex enzyme treatment on the extraction of ZnO-NPs. The same size distribution of ZnO-NPs (50 ± 10 nm, 1 $\mu g\cdot L^{-1}$) was digested in both the control group, where deionized water was added, and treatment group, where a complex enzyme (Macerozyme R-10 enzyme and Carbohydrate-active enzymes) was added after 48 h of enzymatic digestion. The mass concentration and particle size of ZnO-NPs were measured in both the control and treatment groups. Subsequently, the results from both groups were compared. As shown in Fig. 3a and Table S2, the mass concentration recovery of ZnO-NPs and the particle size recovery were both over 85%, and the size distribution of ZnO-NPs after digestion was comparable to those in deionized water as observed by SP-ICP-MS. These results indicated that the complex enzyme did not change the state of ZnO-NPs during the pre-treatment process. Further evidence supporting this came from direct observations in TEM.

Figure 3b compares the TEM image of ZnO-NPs (50 ± 10 nm) subjected to 48 h of enzyme treatment with that of fresh ZnO-NPs. It shows the aggregation of ZnO-NPs and formation of a secondary polymer. Moreover, ZnO-NPs did not possess standard spherical shapes. The TEM data obtained in the particle size range of 50-60 nm was in good agreement with the SP-ICP-MS results. The measurement accuracy of ZnO-NPs sizes was 90-115%, indicating the high reliability of enzyme extraction. However, no significant amounts of ZnO-NPs were detected in rice tissues by TEM at the harvest stage. Note that TEM was mainly used for characterising pure NPs, while the NP contents in the actual plant

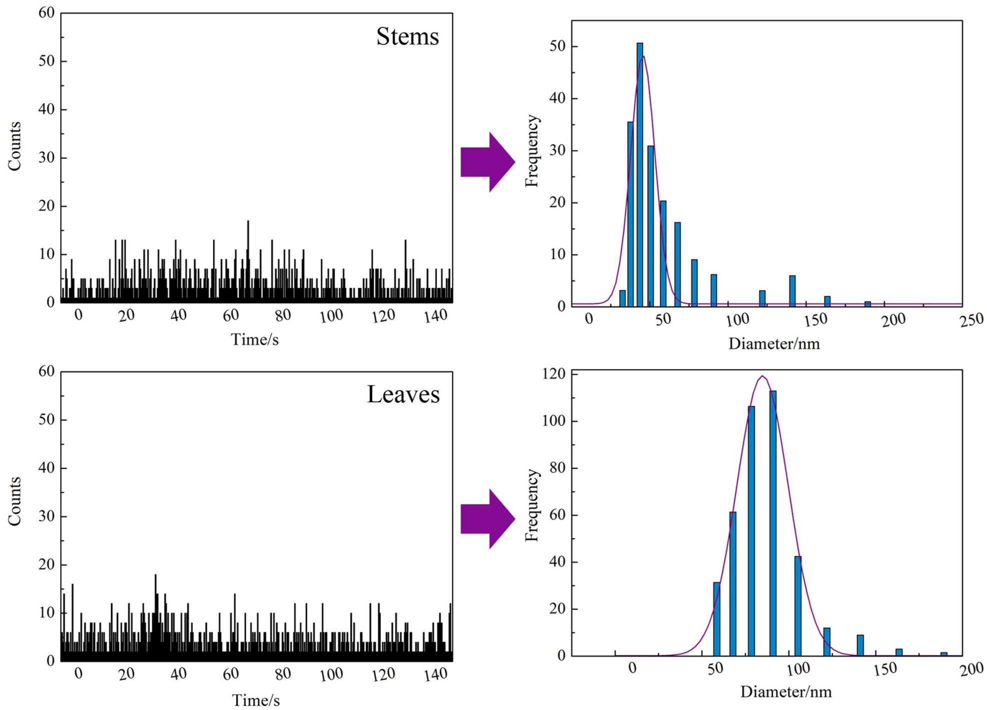

Fig. 4 Original data and size distributions of ZnO-NPs in stems and leaves.

Table 3. Results of single-particle and Zn ion concentration information in different tissues by SP-ICP-MS

Rice tissues	Single-particle data		Zn concentration(mg·kg^{-1})	
	Particle (numbers·g^{-1})	Mean size (nm)	Ck group	Treatment group
Roots	7.41×10^7 (2.9%)	16 ± 2	33.42 ± 2.11	45.82 ± 1.44
Stems	2.14×10^9 (15.8%)	36 ± 10	8.41 ± 1.45	39.24 ± 1.01
Leaves	9.78×10^9 (81.3%)	62 ± 10	6.41 ± 1.78	66.74 ± 1.66
Grains [a]	n.d. [b]	n.d.	5.07 ± 0.46	22.66 ± 0.51

[a] Determined at the harvest stage; [b] not detected.

or environmental samples were extremely low (μg·kg^{-1} to mg·kg^{-1}); therefore, the obtained results were limited by its sensitivity.

ZnO-NPs uptake and transport in rice tissues. The sizes and concentrations of ZnO-NPs in different rice tissues (roots, stems, leaves, and grains) measured using the established method are listed in Table 3. Foliar application of ZnO-NPs increased the total Zn concentrations in the roots, stems, leaves, and grains by 137%, 465%, 1041%, and 447%, respectively, as compared to the control, while the ZnO-NPs absorbed were mainly distributed in leaves (81.3%), followed by stems (15.8%) and roots (2.58%), and no ZnO-NPs was found in rice grains. This demonstrated the feasibility and safety of ZnO-NPs as a foliar Zn fertilizer to match the rice growth. In addition, Zn is also an essential element for humans, its deficient or excessive in food would both affect human health. The Food and Agriculture Organization of the UN (FAO) recommends a minimum of 15 mg·kg^{-1} of Zn in rice,[58] and the Chinese National Agricultural Industry Standards (NY 861-2004) set the maximum limits of Zn in food as 50 mg·kg^{-1}. In this work, the Zn contents in rice grains were 22.66 ± 0.51 mg·kg^{-1}, which matched both the minimum and maximum criteria by these standards.

In plants Zn usually take its effects in ionic forms.[60] According to the ICP-MS data, Zn^{2+} ions were primarily released to leaves rather than other tissues. Khan *et al.* [61] examined the different mechanisms of the enzyme expression acceleration in leaves by NPs. NPs treatment increased the contents of essential enzymes such as hydrolase, phosphorylase, lyase, and invertase, which promoted the dissolution of the original NPs or Zn macro-aggregates within the leaves.[62] The soluble Zn ions were transported by xylem (though hydrostatic pressure) and phloem (though active transport).[63, 64] The results proved that the integral ZnO-NPs not only entered the rice plant through the leave uptake but also partially disassociated as Zn ions, which were subsequently translocated within the plant for the need of rice plant growth.

As shown in Fig. 4, the average diameters of the ZnO-NPs in the leaves and stems, determined from their size distributions, are 62 ± 10 and 36 ± 10 nm, respectively. The ZnO-NPs in the grains is not detectable, and the ZnO-NPs size in the roots is 16 nm, which is close to the limit of detection (LOD) of 14 nm. These results indicated that the ZnO-NPs with size of around 60 nm could be absorbed by rice leaves, and they disassociated to smaller size when transported in stem, or even to be ionic form when transported into the rice grains. Stomata on the leaf surface have been regarded as the main pathway for the uptake of NPs (*e.g.*, Ag, Au, and CeO_2-NPs) by plant leaves;[65] however, inconsistent results have also been reported. For instances, it was observed that foliar applied ZnO-NPs were not absorbed via the leaves, and the association of ZnO-NPs with the rice leaves after rinsing was not improved; similar studies by Li *et al.* [66] also founded that NPs absorption into soybeans was independent of the stomata. Hence, the present literatures did not support the notion that stomatal uptake of the ZnO-NPs into the leaves was the only pathway. The surface of rice leaves is covered by a cuticle, which could be a potential structure for NP uptake in rice plants. Several observations found that hydrophobic NPs with sizes ranging from 5 to 50 nm, such as TiO_2, Ag, and Pb-NPs, could pass through the waxy cuticle.

The NPs were translocated through the leaves to the stems, which was supported using the apoplast for mobility.[67] Remarkably, the cellulose-hemicellulose networks, serving as the framework for the apoplasts, had a pore size of 5-20 nm.[68, 69] Our study observed that the size distribution of the pores in the plant stems were 36 ± 10 nm (> 20 nm). The likely cause for this phenomenon could be the enlargement of pores with the increasing age of the plant. Other Studies have reported that acrylic acid partials (40-50 nm) in grape vine cells induced translocation, with the NPs being trapped between the cell walls of the plant cells. Therefore, the cellulose-hemicellulose system reduced the transport of NPs between the leaves and stems of a plant. In addition to nanoparticle absorption through leaves, Avellan *et al*. [6] found that Au-NPs entered rice plants through root junctions. The first barrier of rice cells contained channels with sizes ranging from 10 to 20 nm.[70, 71] When the size of NPs was smaller than the channel size, they could easily pass the cell and enter the rice plant. In another study, NPs with small sizes of approximately 20 nm and high activity were easily taken up and transported within the roots and grains.[72] However, in this work, ZnO-NPs were barely detected in rice roots and grains, while there is a significant increase in the total zinc concentration in various tissues of the rice plant. With one possible exception, the prepared ZnO-NPs with sizes of approximately 50 to 100 nm used as a foliar fertilizer was bigger than Au-NPs (10-30 nm). Another possibility is that ZnO-NPs, after being absorbed by the leaves, were transported to the stems, and then immobilized. In this process, zinc ions dissolved slowly and were transported to other tissues, including the grains.

Elemental correlation analyses. The elemental correlation analyses were used to explore the relationships between the Zn concentration and the 13 common elements, including beneficial and harmful elements (Table S3). The results indicated a clear correlation between Zn ions from Zn-NPs and other elements in rice. The Zn ion can significantly mitigate the stress responses of heavy metals to plants according to previous literature. In this work, negative correlations between Zn and certain elements in rice, indicating that Zn can reduce the concentration of these elements throughout the rice plant. Specifically, negative correlations were found between the Zn and some elements (i.e., Cd, As, Fe, and Pb), particularly As ($R= -0.615$, $P= 0.009$) and Pb ($R= -0.851$, $P= 0.008$). As, Cd, and Pb are non-essential and they can cause the leaching of nutrients and inhibit photosynthesis in rice. Hence, Zn might have the potential to mitigate the stress caused by heavy metals. However, a positive correlation was existed between Zn and Mg ($R= 0.769$, $P= 0.036$). Among those mineral nutrients, Mg is closely related to the photosynthesis of plants and is influenced by environmental perturbations. Notably, Zn not only can remit the uptake of heavy metals but also improves the resilience to environmental stressors.

Based on the correlation analysis, PCA was applied to perform an in-depth analysis, reducing the dimensionality of data. The different elements (containing Zn, Mg, Fe, Pb, As, and Ca) levels could be affected the spatial distribution of the studied elements in these biological systems (Fig. 5a). All the elements were associated with PC1. It is universal that the accumulation of inorganic elements shows significantly between tissues and plant types. Zn sprayed on leaves will affect the absorption of Zn from the soil by rice.[73] As shown in Fig. 5b, the two mains of PCs (PC1 and PC2) explain 56.6% and 11.7% of the variance, respectively. The primary differentiation is observed between the roots and grains. The results exhibited that the roots had minimal effect on the ionic concentrations from Zn ions. The foliar application of Zn had an impact on the ion concentrations in the leaves, stems, and grains. Therefore, the increase in Zn concentrations in the roots cannot be attributed to the foliar Zn application alone. This phenomenon may be attributed to the fact that the Zn sprayed on the leaves fell into the soil and be absorbed by the roots. Considering the earlier discussion on Zn ion transport in rice, we can confirm that reverse ion transport is almost non-existent from leaf to root.

CONCLUSION

In this work, we developed a method using a complex enzyme system for the extraction of ZnO-NPs in plant tissues without causing dissolution or aggregation. The compound enzyme digestion system, followed by SP-ICP-MS technology, could be used to simultaneously detect, and quantify the uptake and transport efficiency of ZnO-NPs in different plant tissues. We studied the characteristics of uptake of ZnO-NPs by rice and their transportation in rice plants following foliar application of ZnO-NPs. The results proved the feasibility and safety of ZnO-NPs as a foliar Zn fertilizer to rice. The established method overcomes current technique challenges by accurately determining the concentration and unique characteristics of ZnO-NPs in complex matrix. This significant advancement will greatly contribute to the risk assessment of engineered NPs in plants.

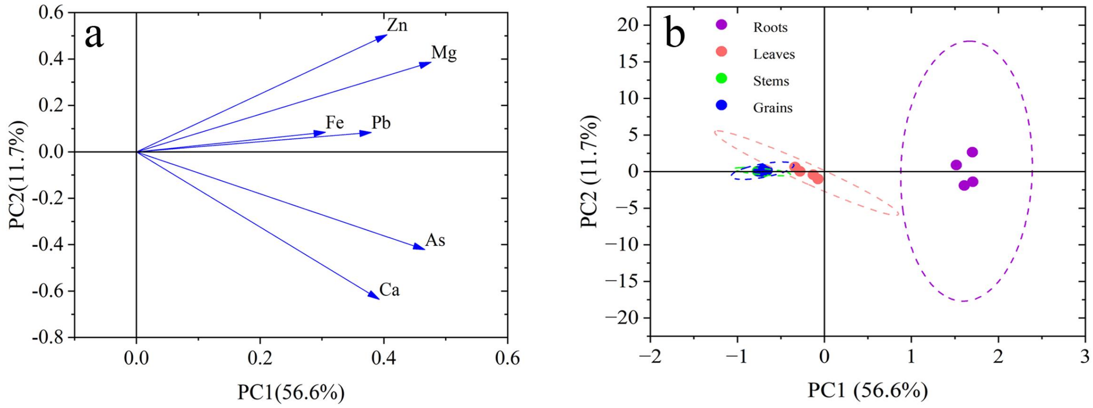

Fig. 5 PCA score plot for elements concentration level in different tissues (a). Score/loading plots of the first two PCs obtained from PCA applied to the 4 datasets corresponding to each element. The samples are shown according to the specific part of the plant: root (purple), leaf (orange), stem (green) and grain (blue) (b). The confidence interval was 0.95.

ASSOCIATED CONTENT

The supporting information (Fig. S1 and Table S1-S3) is available at www.at-spectrose.com/as/home.

AUTHOR INFORMATION

Shiqiang Wei holds a Ph.D. degree from Swedish Agricultural University (Swedish) and is currently a full professor in Southwest University. His major research interest is in the field of environmental science, specifically in the control and management of non-point source pollution in farmland and the processes of soil pollution and remediation. Shi-qiang Wei served as the Principal Investigator for over 30 research projects and received 8 awards at the national and provincial levels for scientific and technological achievements. He is author or co-author of over 200 articles published in peer-reviewed scientific journals. He has supervised the graduation of more than 20 doctoral students and over 80 master's students, achieving fruitful results in research, talent development, and other areas.

Corresponding Author

* S. Q. Wei

Email address: sqwei@swu.edu.cn

Notes

The authors declare no competing financial interest.

ACKNOWLEDGMENTS

This work was supported by the National Nature Science Foundation of China (42177012) and the Open Fund of Key Laboratory of Testing and Tracing of Rare Earth Products for State Market Regulation (TTREP2022YB01). We thank Dr. Lan Yang (Southwest University) for providing valuable technical assistance using the ICP-MS.

REFERENCES

1. M. Nikolic, N. Nikolic, L. Kostic, J. Pavlovic, P. Bosnic, N. Stevic, J. Savic, and N. Hristov, *Sci. Total Environ.*, 2016, **553**, 141-148. https://doi.org/10.1016/j.scitotenv.2016.02.102
2. M.-C. Affholder, D. J. Weiss, M. Wissuwa, S. E. Johnson-Beebout, and G. J. D. Kirk, *Plant, Cell Environ.*, 2017, **40**, 3018-3030. https://doi.org/10.1111/pce.13069
3. M. S. Akther, U. Das, S. Tahura, S. A. Prity, M. Islam, and A. H. Kabir, *Sci. Hortic.*, 2020, **273**, 109624. https://doi.org/10.1016/j.scienta.2020.109624
4. X. Gao, A. Kundu, V. Bueno, A. A. Rahim, and S. Ghoshal, *Environ. Sci. Technol.*, 2021, **55**, 13551-13560. https://doi.org/10.1021/acs.est.1c00447
5. H. Cui, S. Tang, S. Huang, L. Lei, Z. Jiang, L. Li, and S. Wei, *Sci. Total Environ.*, 2022, **860**, 160307. https://doi.org/10.1016/j.scitotenv.2022.160307
6. A. Avellan, J. Yun, Y. Zhang, E. Spielman-Sun, J. M. Unrine, J. Thieme, J. Li, E. Lombi, G. Bland, and G. V. Lowry, *ACS Nano*, 2019, **13**, 5291-5305. https://doi.org/10.1021/acsnano.8b09781
7. M. Kah, D. Navarro, R. S. Kookana, J. K. Kirby, S. Santra, A. Ozcan, and S. Kabiri, *Environ. Chem.*, 2019, **16**, 401-410. https://doi.org/10.1071/EN18279
8. T. Eichert, A. Kurtz, U. Steiner, and H. E. Goldbach, *Physiol. Plant.*, 2008, **134**, 151-160. https://doi.org/10.1111/j.1399-3054.2008.01135.x
9. A. B. Bombo, A. E. S. Pereira, M. G. Lusa, E. de Medeiros Oliveira, J. L. de Oliveira, E. V. R. Campos, M. B. de Jesus, H. C. Oliveira, L. F. Fraceto, and J. L. S. Mayer, *J. Agric. Food. Chem.*, 2019, **67**, 4453-4462. https://doi.org/10.1021/acs.jafc.9b00806

10. M. Zeyrek Ongun, S. Oguzlar, U. Kartal, M. Yurddaskal, and O. Cihanbegendi, *Solid State Sci.*, 2021, **122**, 106772. https://doi.org/10.1016/j.solidstatesciences.2021.106772

11. A. Avellan, J. Yun, B. P. Morais, E. T. Clement, S. M. Rodrigues, and G. V. Lowry, *Environ. Sci. Technol.*, 2021, **55**, 13417-13431. https://doi.org/10.1021/acs.est.1c00178

12. E. Gerber, A. Y. Romanchuk, I. Pidchenko, L. Amidani, A. Rossberg, C. Hennig, G. B. M. Vaughan, A. Trigub, T. Egorova, S. Bauters, T. Plakhova, M. O. J. Y. Hunault, S. Weiss, S. M. Butorin, A. C. Scheinost, S. N. Kalmykov, and K. O. Kvashnina, *Nanoscale*, 2020, **12**, 18039-18048. https://doi.org/10.1039/D0NR03767B

13. A. Bahadoran, M. Khoshnoudi Jabarabadi, Z. Hameed Mahmood, D. Bokov, B. Jushi Janani, and A. Fakhri, *Spectrochim. Acta A*, 2022, **268**, 120636. https://doi.org/10.1016/j.saa.2021.120636

14. J. Iqbal, B. A. Abbasi, T. Mahmood, S. Kanwal, R. Ahmad, and M. Ashraf, *J. Mol. Struct.*, 2019, **1189**, 315-327. https://doi.org/10.1016/j.molstruc.2019.04.060

15. B. Meermann and V. Nischwitz, *J. Anal. At. Spectrom.*, 2018, **33**, 1432-1468. https://doi.org/10.1039/C8JA00037A

16. Y. F. Wu, S. S. Liu, Y. W. Xu, L. Yu, Z. Yang, H. H. Wang, and Y. S. Guo, *Atom. Spectrosc.*, 2021, **42**, 160-165. https://doi.org/10.46770/AS.2020.196

17. D. Yildiz, *Atom. Spectrosc.*, 2021, **42**, 197-202. https://doi.org/10.46770/AS.2021.026

18. L. X. Kuang, J. Y. Nie, J. Y. Zhang, G. F. Xu, J. Li, Y. Cheng, Y. M. Shen, and F. Saqi, *Atom. Spectrosc.*, 2021, **42**, 91-98. https://doi.org/10.46770/AS.2021.004

19. A. C. Sahayam, G. Venkateswarlu, and S. Thangavel, *Atom. Spectrosc.*, 2021, **42**, 32-35. https://doi.org/10.46770/AS.2020.183

20. N. S. Medvedev, N. A. Orlov, and A. I. Saprykin, *Atom. Spectrosc.*, 2022, **43**, 430-436. https://doi.org/10.46770/AS.2022.248

21. D. C. He, X. F. Yang, R. Zhang, T. Xia, Y. Liu, S. C. Yang, K. Hu, Z. G. Li, and X. D. Wen, *Atom. Spectrosc.*, 2022, **43**, 246-254. https://doi.org/10.46770/AS.2022.100

22. R. A. Althobiti and D. Beauchemin, *Atom. Spectrosc.*, 2021, **42**, 271-277. https://doi.org/10.46770/AS.2020.708

23. Y. Wu, D. M. Huang, T. Feng, L. L. Jin, D. Xiong, J. Yu, Q. Xu, R. M. Huang, S. H. Hu, *Atom. Spectrosc.*, 2021, **42**, 374-382. https://doi.org/10.46770/AS.2021.906

24. Y. B. Zhu, T. Ariga, K. Nakano, and Y. Shikamori, *Atom. Spectrosc.*, 2021, **42**, 299-309. https://doi.org/10.46770/AS.2021.710

25. S. Xing, M. Y. Luo, N. Yuan, D. Q. Liu, Y. Yang, X. X. Dai, W. C. Zhang, and N. Chen, *Atom. Spectrosc.*, 2021, **42**, 62-70. https://doi.org/10.46770/AS.2021.011

26. Y. N. Gotame, V. Gandolfi, and D. Beauchemin, *Atom. Spectrosc.*, 2022, **43**, 443-449. https://doi.org/10.46770/AS.2022.229

27. Q. Zhao and Q. H. Guo, *Atom. Spectrosc.*, 2022, **43**, 230-235. https://doi.org/10.46770/AS.2022.032

28. Z. Q. Deng, J. Y. Hu, R. Liu, and Y. Lv, *Atom. Spectrosc.*, 2022, **43**, 201-206. https://doi.org/10.46770/AS.2021.1013

29. O. V. Kuznetsova, and A. R. Timerbaev, *Atom. Spectrosc.*, 2021, **42**, 85-90. https://doi.org/10.46770/AS.2021.005

30. Y. Hua, S. Zhang, H. Min, J.-Y. Li, X.-H. Wu, D. Sheng, X.-B. Cui, Y.-J. Chen, C. Li, H.-Z. Lian, S. Liu, *Atom. Spectrosc.*, 2021, **42**, 217-226. https://doi.org/10.46770/AS.2021.027

31. A. Kierulf, C. Pytyck, and D. Beauchemin, *Atom. Spectrosc.*, 2021, **42**, 365-373. https://doi.org/10.46770/AS.2021.724

32. H. E. Pace, N. J. Rogers, C. Jarolimek, V. A. Coleman, C. P. Higgins, and J. F. Ranville, *Anal. Chem.*, 2011, **83**, 9361-9369. https://doi.org/10.1021/ac201952t

33. E. Bolea-Fernandez, D. Leite, A. Rua-Ibarz, L. Balcaen, M. Aramendía, M. Resano, and F. Vanhaecke, *J. Anal. At. Spectrom.*, 2017, **32**, 2140-2152. https://doi.org/10.1039/C7JA00138J

34. P. P. Chang, L. N. Zheng, B. Wang, M. L. Chen, M. Wang, J. H. Wang, and W. Y. Feng, *Atom. Spectrosc.*, 2022, **43**, 255-265. https://doi.org/10.46770/AS.2022.108

35. J. H. Liu, L. N. Zheng, J. W. Wei, X. Li, M. L. Cheng, M. Wang, J. H. Wang, and W. Y. Feng, *Atom. Spectrosc.*, 2021, **42**, 114-119. https://doi.org/10.46770/AS.2021.102

36. H. Z. Sun and Y. F. Li, *Atom. Spectrosc.*, 2021, **42**, 227-230. https://doi.org/10.46770/AS.2021.108

37. M. Y. Pan, Y. Zang, X. R. Zhou, Y. Li. Lu, J. P. Xiong, H. M. Li, and L. X. Feng, *Atom. Spectrosc.*, 2021, **42**, 262-270. https://doi.org/10.46770/AS.2021.104

38. E. Bolea-Fernandez, D. Leite, A. Rua-Ibarz, T. Liu, G. Woods, M. Aramendia, M. Resano, and F. Vanhaecke, *Anal. Chim. Acta*, 2019, **1077**, 95-106. https://doi.org/10.1016/j.aca.2019.05.077

39. L. Fréchette-Viens, M. Hadioui, and K. J. Wilkinson, *Talanta*, 2019, **200**, 156-162. https://doi.org/10.1016/j.talanta.2019.03.041

40. W.-J. Wei, L. Li, Y.-P. Gao, Q. Wang, Y.-Y. Zhou, X. Liu, and Y. Yang, *Sci. Total Environ.*, 2021, **777**, 146038. https://doi.org/10.1016/j.scitotenv.2021.146038

41. S. Laughton, A. Laycock, G. Bland, F. von der Kammer, T. Hofmann, E. A. Casman, and G. V. Lowry, *Anal. Bioanal. Chem.*, 2021, **413**, 299-314. https://doi.org/10.1007/s00216-020-03014-8

42. F.-B. Wu, J. Dong, Q. Q. Qian, and G.-P. Zhang, *Chemosphere*, 2005, **60**, 1437-1446. https://doi.org/10.1016/j.chemosphere.2005.01.071

43. F. Laborda, A. C. Gimenez-Ingalaturre, E. Bolea, and J. R. Castillo, *Spectrochim. Acta B*, 2020, **169**, 105883. https://doi.org/10.1016/j.sab.2020.105883

44. A. C. Gimenez-Ingalaturre, K. Ben-Jeddou, J. Perez-Arantegui, M. S. Jimenez, E. Bolea, and F. Laborda, *Anal. Bioanal. Chem.*, 2023, **415**, 2101-2112. https://doi.org/10.1007/s00216-022-04215-z

45. M. Hadioui, G. Knapp, A. Azimzada, I. Jreije, L. Frechette-Viens, and K. J. Wilkinson, *Anal. Chem.*, 2019, **91**, 13275-13284. https://doi.org/10.1021/acs.analchem.9b04007

46. V. Geertsen, P. Lemaitre, M. Tabarant, and F. Chartier, *J. Anal. At. Spectrom.*, 2012, **27**, 146-158. https://doi.org/10.1039/C1JA10255A

47. N. Braukmüller, F. Wombacher, A. Bragagni, and C. Münker, *Geostand. Geoanal. Res.*, 2020, **44**, 733-752. https://doi.org/10.1111/ggr.12352

48. C. A. Hartwig, I. G. Toralles, M. G. Crizel, A. L. Hermes Muller, R. S. Picoloto, E. M. Moraes Flores, and M. F. Mesko, *Anal. Methods*, 2014, **6**, 7540-7546. https://doi.org/10.1039/C4AY00974F

49. T. N. Akbaba, N. Ertas, and O. Alp, *Anal. Lett.*, 2022, **55**, 580-595. https://doi.org/10.1080/00032719.2021.1950166

50. M. D. Montaño, B. J. Majestic, Å. K. Jämting, P. Westerhoff, and J. F. Ranville, *Anal. Chem.*, 2016, **88**, 4733-4741. https://doi.org/10.1021/acs.analchem.5b04924

51. K. Ding, S. Liang, C. Xie, Q. Wan, C. Jin, S. Wang, Y.-T. Tang, M. Zhang, and R. Qiu, *Anal. Chem.*, 2022, **94**, 10745-10753. https://doi.org/10.1021/acs.analchem.2c01379
52. S. Lee, X. Bi, R. B. Reed, J. F. Ranville, P. Herckes, and P. Westerhoff, *Environ. Sci. Technol.*, 2014, **48**, 10291-10300. https://doi.org/10.1021/es502422v
53. M. D. Montaño, J. W. Olesik, A. G. Barber, K. Challis, and J. F. Ranville, *Anal. Bioanal. Chem.*, 2016, **408**, 5053-5074. https://doi.org/10.1007/s00216-016-9676-8
54. D. Mozhayeva and C. Engelhard, *J. Anal. At. Spectrom.*, 2019, **34**, 1571-1580. https://doi.org/10.1039/C9JA00042A
55. T. E. Lockwood, R. Gonzalez de Vega, and D. Clases, *J. Anal. At. Spectrom.*, 2021, **36**, 2536-2544. https://doi.org/10.1039/D1JA00297J
56. F. Laborda, J. Jiménez-Lamana, E. Bolea, and J. R. Castillo, *J. Anal. At. Spectrom.*, 2013, **28**, 1220-1232. https://doi.org/10.1039/C3JA50100K
57. J. Ma, H. Alshaya, M. K. Okla, Y. A. Alwasel, F. Chen, M. Adrees, A. Hussain, S. Hameed, and M. J. Shahid, *Front. Plant Sci.*, 2022, **13**, 876119. https://doi.org/10.3389/fpls.2022.876119
58. J. R. Lupien, *Am. J. Clin. Nutr.*, 1994, **59**, 269S-270S. https://doi.org/10.1093/ajcn/59.1.269S
59. M. Faizan, J. A. Bhat, K. Hessini, F. Yu, and P. Ahmad, *Ecotoxicol. Environ. Saf.*, 2021, **220**, 112401. https://doi.org/10.1016/j.ecoenv.2021.112401
60. S. Sheikhnazari, Y. Niknezhad, H. Fallah, and D. Barari Tari, *Gesunde Pflanzen*, 2023, **75**, 211-221. https://doi.org/10.1007/s10343-022-00691-6
61. M. R. Khan, V. Adam, T. F. Rizvi, B. Zhang, F. Ahamad, I. Jośko, Y. Zhu, M. Yang, and C. Mao, *Small*, 2019, **15**, 1901794. https://doi.org/10.1002/smll.201901794
62. K. Kozak, A. Papierniak, A. Barabasz, M. Kendziorek, M. Palusińska, L. E. Williams, and D. M. Antosiewicz, *Environ. Exp. Bot.*, 2019, **157**, 69-78. https://doi.org/10.1016/j.envexpbot.2018.09.020
63. L. Lu, S. Tian, J. Zhang, X. Yang, J. M. Labavitch, S. M. Webb, M. Latimer, and P. H. Brown, *New Phytol.*, 2013, **198**, 721-731. https://doi.org/10.1111/nph.12168
64. S. Mu, N. Yamaji, A. Sasaki, L. Luo, B. Du, J. Che, H. Shi, H. Zhao, S. Huang, F. Deng, Z. Shen, M. L. Guerinot, L. Zheng, and J. F. Ma, *Plant J.*, 2021, **105**, 786-799. https://doi.org/10.1111/tpj.15073
65. H. Park, S. Park, Y.-H. Yang, and K.-Y. Choi, *Crit. Rev. Biotechnol.*, 2021, **41**, 879-901. https://doi.org/10.1080/07388551.2021.1892579
66. C. Li, P. Wang, E. Lombi, M. Cheng, C. Tang, D. L. Howard, N. W. Menzies, and P. M. Kopittke, *J. Exp. Bot.*, 2018, **69**, 2717-2729. https://doi.org/10.1093/jxb/ery085
67. I. Gentzel, L. Giese, G. Ekanayake, K. Mikhail, W. Zhao, J.-C. Cocuron, A. P. Alonso, and D. Mackey, *Cell Host Microbe*, 2022, **30**, 502-517.e4. https://doi.org/10.1016/j.chom.2022.03.017
68. X. Chen, Y. Li, L. Jiang, B. Hu, L. Wang, S. An, and X. Zhang, *Sci. Total Environ.*, 2021, **753**, 141979. https://doi.org/10.1016/j.scitotenv.2020.141979
69. F. Schwab, G. Zhai, M. Kern, A. Turner, J. L. Schnoor, and M. R. Wiesner, *Nanotoxicology*, 2016, **10**, 257-278. https://doi.org/10.3109/17435390.2015.1048326
70. J. Zhu, J. Wang, X. Zhan, A. Li, J. C. White, J. L. Gardea-Torresdey, and B. Xing, *ACS Sustain. Chem. Eng.*, 2021, **9**, 11556-11564. https://doi.org/10.1021/acssuschemeng.1c04080
71. T. C. Thounaojam, T. T. Meetei, Y. B. Devi, S. K. Panda, and H. Upadhyaya, *Acta Physiol. Plant.*, 2021, **43**, 136. https://doi.org/10.1007/s11738-021-03307-0
72. Y. Su, V. Ashworth, C. Kim, A. S. Adeleye, P. Rolshausen, C. Roper, J. White, and D. Jassby, *Environ. Sci-Nano.*, 2019, **6**, 2311-2331. https://doi.org/10.1039/C9EN00461K
73. H. Xia, Y. Xue, D. Liu, W. Kong, Y. Xue, Y. Tang, J. Li, D. Li, and P. Mei, *Front. Plant Sci.*, 2018, **9**, 677. https://doi.org/10.3389/fpls.2018.00677